OPEN ACCESS
Journal of Multidisciplinary Applied Natural Science Vol. 4 No. 1 (2024) https://doi.org/10.47352/jmans.2774-3047.192
Check for updates
Research Article

Enhancing Photocatalytic Activity of Bismuth Ferrite ($BiFeO_3$) via Gadolinium and Copper Doping: A Sol-Gel Synthesis and Characterization Study

Beerelli Rajitha* and Padma Suvarna

Received : September 9, 2023	Revised : September 25, 2023	Accepted : September 25, 2023	Online : October 3, 2023

Abstract
In this current research work, the sol-gel method was employed to synthesise, characterize and evaluate the photocatalytic activity of bismuth ferrite (BiFeO3, BFO) doped with two distinctive components consisting of a rare earth element Gadolinium (Gd) and a transition metal Copper (Cu). The dopant concentrations were systematically varied with different weight percentages (wt.%) denoted as Bi1-xGdxFe1-yCuyO3 (where 'x' = 0.10, 0.15 and 0.20 wt.%, where 'y' = 0.05, 0.10, and 0.15 wt.%). Subsequently, characterizations of the prepared samples were conducted using an array of cutting-edge analytical techniques including X-ray diffraction (XRD), filed emission scanning electron microscopy (FE-SEM), energy dispersive X-ray analysis (EDAX), and transmission electron microscopy (TEM). The XRD analysis results indicated that the presence of small impurity peaks was found in both Gd-doped BFO and GdCu-doped BFO. The FE-SEM and TEM results provided confirmation that the material was observed as a spherical shape, and the elemental compositions were also confirmed through EDAX analysis. The photocatalytic degradation of Rhodamine B dye under the influence of visible light irradiation was carried out and the results revealed varying degradation times, specifically, for Gd and Cu-doped BFO (Gd and Cu = 0.1 wt.%) achieved almost 98% degradation occurred in 30 minutes.

Keywords: bismuth ferrite, sol–gel method, rare earth material, transition metal, photocatalytic, Rhodamine B.

1. INTRODUCTION

Due to extensive industrialization, urbanization, and rising populations, the provision of clean water has become a global concern. The primary source of water pollution is the improper management of industrial wastewater disposal in freshwater streams [1][2]. For industrial use, many organic dyes are created and then discarded as colorful effluents. Qu et al. [3] reported many industries released waste containing dye solutions, which resulted in water pollution. A significant source of colored effluents is the textile industry, and each year almost 200 billion liters of waste are released into the environment [4]. Dyes are a problem since the families of chemical compounds are also harmful to living organisms and are regarded as dangerous contaminants [5]. Even at very low concentrations, these dangerous color molecules poison the waters around us. Therefore, removing these colors from water is essential. To control this issue, several techniques are there including ion exchange removal [6], catalytic reduction [7], ozonation [8], biological/aerobic treatment [9], adsorption [10], membrane filtration [11], and photocatalytic degradation [12][13]. Research in the field of photocatalysis has increased significantly over the last several years. Due to its capacity to remove toxins from water pollutants by employing nano-sized metal oxides as catalysts, photocatalysis has recently attracted a lot of interest as a viable environmental remediation approach [14]-[16].

For several applications, different metal oxide nanoparticles have been employed including the photodegradation of dye solutions and purification of contaminated water [17]-[22]. Bismuth ferrite (BFO) is regarded as an interesting photocatalyst for the degradation of a wide range of contaminants in various chemical processes, due to its high catalytic mobility, high stability, low toxicity, and less expensive, as well as its relatively low band gap value [23]-[27]. The photocatalytic application of pure BFO is not satisfying because of its favorable conditions for excited electron and hole recombination. However, it can be controlled by doping with suitable materials. The distortion of the structure and ionic radius of dopant ions enhance the properties of BFO. The proper copper (Cu) concentration in Cu-BFO was found to be 1.0

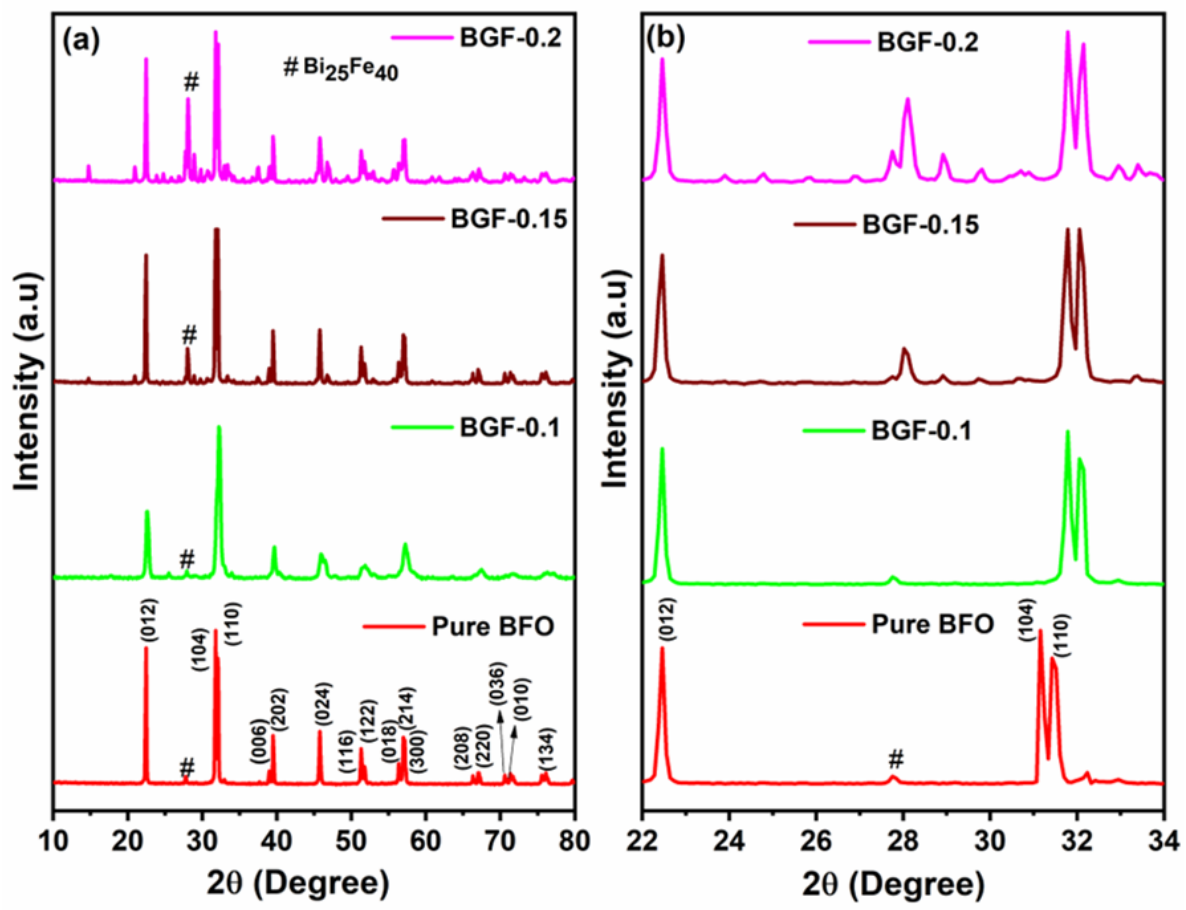

Figure 1. (a) Full XRD pattern (10–80°) and (b) magnified peaks (22–34°) of pure BFO, BGF-0.1, BGF-0.15, and BGF-0.2.

mol%, which showed the highest photocatalytic activity for degrading methyl orange aqueous solution under visible light irradiation after 120 min [28]. Jie et al. reported that the 0.2 Cu presented in BFO yielded prominent catalytic performance for phenol degradation in 120 min [29]. A maximum degradation efficiency was also obtained for the gadolinium (Gd)-doped BFO with 5% Gd after 60 min for Rhodamine B (RhB) [30]. The low concentration of Gd doping below 0.1 could significantly increase the photocatalytic activity highest degradation observed in 120 min [27].

In this present work, we have synthesized pure and two different metal ions (Cu and Gd) doped BFO using the sol-gel method. The enhanced photocatalytic properties of BFO and GdCu-doped BFO for the RhB dye degradation under visible light were observed and discussed. To the best of our knowledge, there were few reports in the literature on both rare earth and transition metal ions doped BFO and comparisons of their various properties.

2. MATERIALS AND METHODS

2.1. Materials and Chemicals

Iron(III) nitrate nonahydrate ($Fe(NO_3)\cdot 9H_2O$), nitric acid (HNO_3), bismuth(III) nitrate pentahydrate ($Bi(NO_3)_3\cdot 6H_2O$), tartaric acid ($C_4H_4O_6$), gadolinium(III) nitrate hexahydrate ($Gd(NO_3)\cdot 6H_2O$), copper(II) nitrate trihydrate ($Cu(NO_3)\cdot 3H_2O$) were in analytical-grade chemicals from Sigma Aldrich and used throughout the experiment.

2.2. Synthesis Procedure

The pure BFO, Gd-, and Cu-doped BFO samples with different (wt.%) synthesized by sol-gel method. For comparison study primarily the pure BFO is prepared in the following procedure.

2.2.1. Synthesis of Pure BFO

First step, 1.91 g of $Fe(NO_3)\cdot 9H_2O$ was dissolved in 50 mL of distilled water with continuous stirring. Then 10 mL of HNO_3 was

added dropwise to the above solution for the adjustment of pH to 1. In the next step, 2.42 g of Bi $(NO_3)_3 \cdot 6H_2O$ and 25 mL of $C_4H_4O_6$ were added. After some time, a light yellowish transparent solution formed. The gel was created by heating the resulting solution to 90 °C for 60 min and the temperature was then raised to 180 °C (or more) to trigger solvent evaporation and the creation of powder. The obtained brown powder was crushed with a mortar and pestle and annealed for 3 h at 600 °C. The prepared pure $BiFeO_3$ is labeled as BFO.

2.2.2. Synthesis of Gd-doped BFO

In the second step, Gd doped BFO with different (wt.%), i.e., $Bi_{1-x}Gd_xFeO_3$ (where x = 0.10, 0.15 and 0.20 wt.%) prepared in the following procedure. As much as 1.91 g of $Fe(NO_3) \cdot 9H_2O$ was dissolved at first in 50 mL of distilled water while being continuously stirred. To get a pH value of 1, 10 mL of HNO_3 was added to the above solution. In the next step, 2.17 g of $Bi(NO_3)_3 \cdot 6H_2O$ and 0.225 g (0.1 wt.%) of $Gd(NO_3) \cdot 6H_2O$ were added to the resultant solution. Then, a dropwise addition of 25 mL of $C_4H_4O_6$ was added until a clear solution had formed. The solution was heated to 90 °C for 1 h to form the gel. To promote solvent evaporation and powder production, the temperature was raised to 180 °C (or more). The obtained powder was then crushed and annealed at 600 °C for 3 h. The prepared Gd doped BFO, i.e., $Bi_{1-x}Gd_xFeO_3$ (where x = 0.10; $Bi_{0.9}Gd_{0.1}FeO_3$) labeled as BGF-0.1. In a similar method, other two Gd-doped BFO samples were also prepared (x = 0.15 wt.%; $Bi_{0.85}Gd_{0.15}FeO_3$ and 0.20 wt.%; $Bi_{0.8}Gd_{0.25}FeO_3$). Prepared samples labeled as BGF-0.15 and BGF-0.2.

2.2.3. Synthesis of GdCu-doped BFO

In the third step, Gd (0.1 wt.%) kept as constant and Cu-doped with different (wt.%) i.e., $Bi_{0.9}Gd_{0.1}Fe_{1-y}Cu_yO_3$ (where y= 0.05, 0.10, and 0.15 wt.%) and applied same above synthesis procedure. The prepared GdCu-doped BFO, i.e., $Bi_{0.9}Gd_{0.1}Fe_{0.95}Cu_{0.05}O_3$, $Bi_{0.9}Gd_{0.1}Fe_{0.9}Cu_{0.1}O_3$, and $Bi_{0.9}Gd_{0.1}Fe_{0.85}Cu_{0.15}O_3$ are labelled as BGFC-0.05, BGFC-0.1, and BGCF-0.15, respectively.

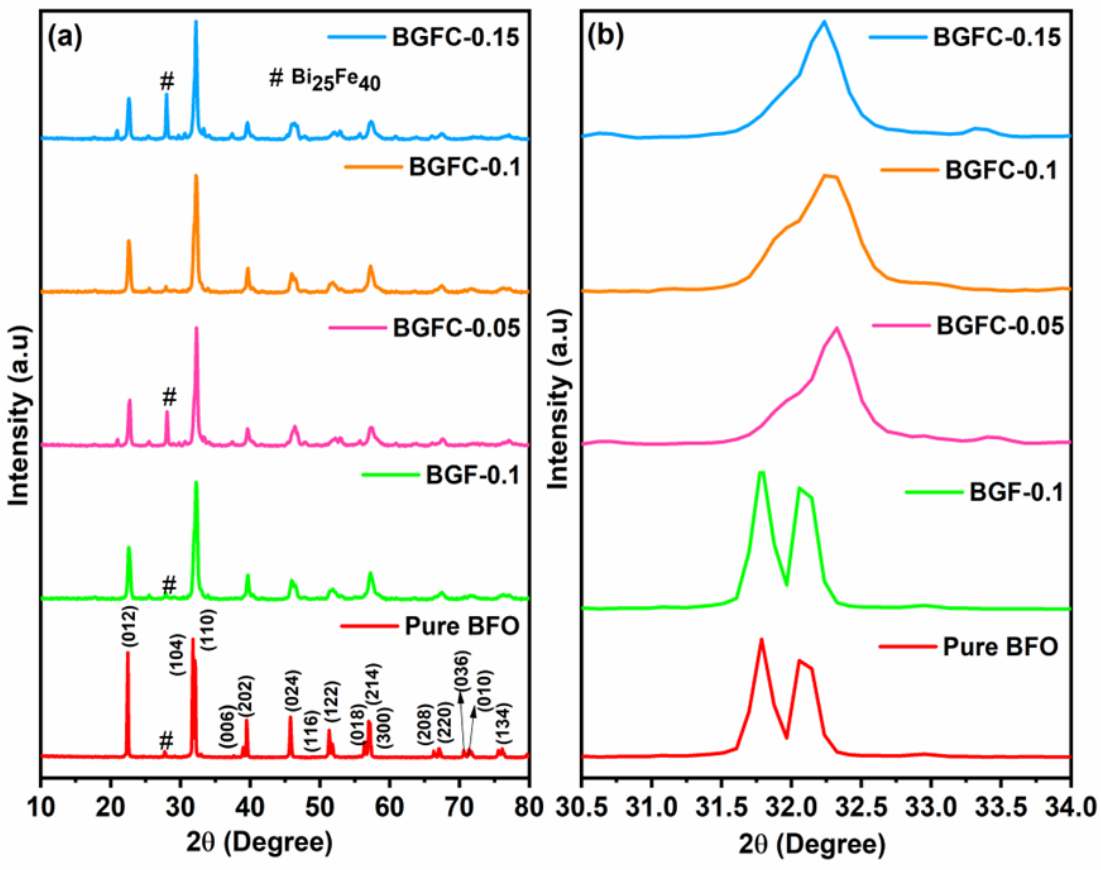

Figure 2. (a) Full XRD pattern (10–80°) and (b) magnified peaks (22–34°) of pure BFO, BGF-0.1, BGFC-0.05, BGFC-0.1, and BGFC-0.15.

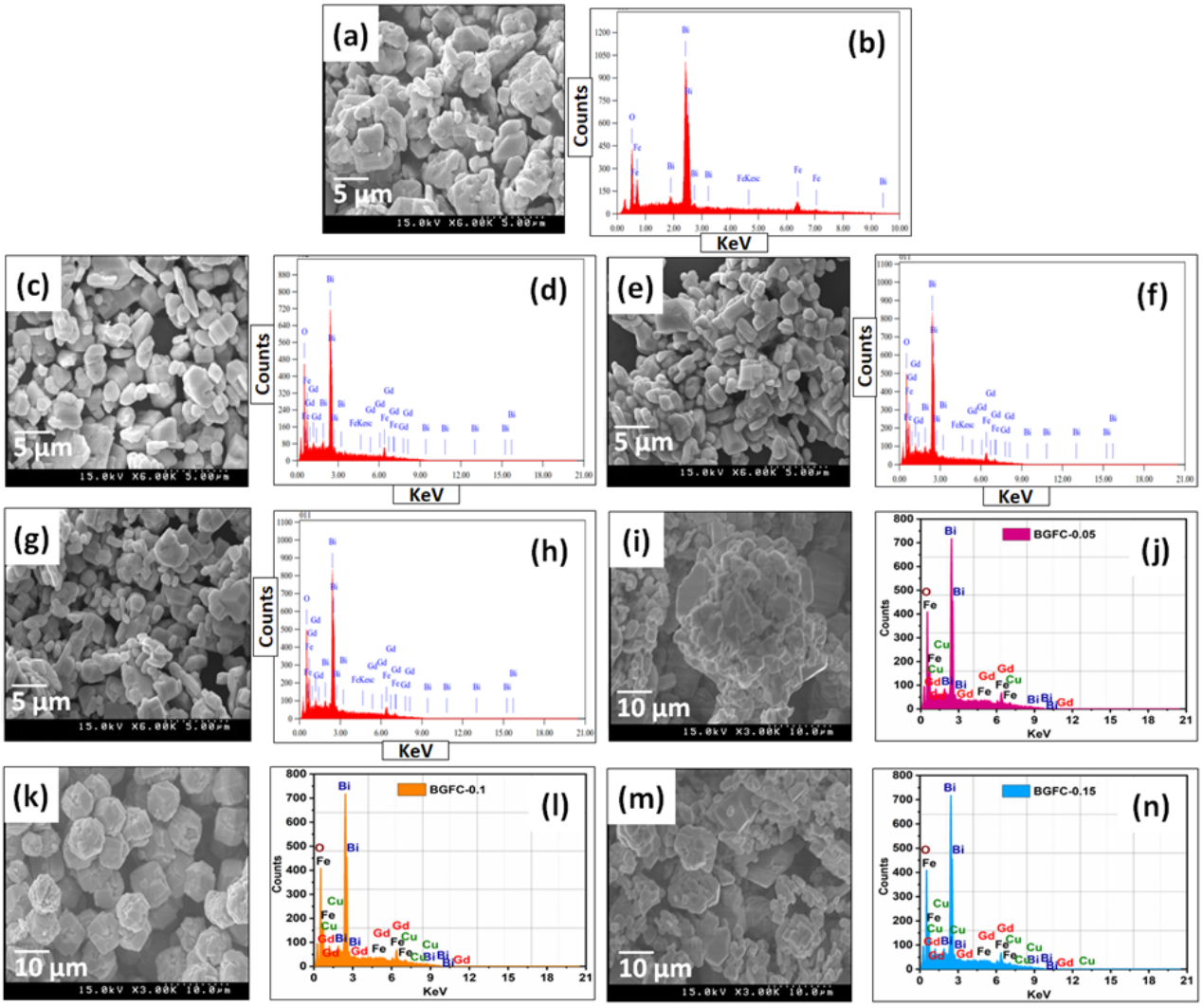

Figure 3. FE-SEM and EDAX results of (a-h) pure BFO, BGF-0.1, BGF-0.15, BGF-0.2, (i-n) BGFC-0.05, BGFC-0.1, and BGFC-0.15.

2.3 Characterization Techniques

The synthesized samples were characterized including X-ray diffraction (XRD, XRD-Model. No: Bruker D8 advance) to determine the crystal structure and phase composition, filed emission scanning electron microscopy (FE-SEM, Model No. JEOL 7600) to visualize the surface morphology, energy dispersive X-ray analysis (EDAX) to ascertain the elemental composition, and transmission electron microscopy (TEM, Model No. JEOLJEM-200X) to probe the microstructure at the nanoscale.

3. RESULTS AND DISCUSSIONS

3.1. Structural Analysis

The XRD pattern of synthesized pure BFO and Gd-doped BFO (BGF-0.1, BGF-0.15, and BGF-0.2) samples is shown in Figure 1. The diffraction patterns of the Gd-doped BFO samples (BGF-0.1, BGF-0.15, and BGF-0.2) are similar to the pure BFO pattern along with the presence of additional minor peaks indicated as secondary impurities. Figure 1(a) reveals that the Gd-doped samples at various weight percentages exhibit new peaks at glancing angles (27.91° and 32.65°). These peaks may arise from the monoclinic structure of Gd_2O_3. Although Gd^{3+} ions maintain the basic crystal structure (tetragonal). From the magnified XRD patterns in the vicinity of 2θ = 22 to 34° (Figure 1 (b)), it becomes apparent that the Gd dopant caused a shift in the separated (104) and (110) planes towards higher angles. This shift is attributed to the substitution of Gd ions (with a 9.38 Å radius) for Bi^{3+} ions (with a 10.30 Å radius) in the BFO structure [31].

Further work, keeping Gd (0.1 wt.%) constant and doping of Cu with different (wt.%) (BGFC-0.05, BGFC-0.1 BGFC-0.15) samples as shown in Figure 2(a). The doped samples exhibited similar patterns to pure BFO and BGF-0.1 However, the impurity peak was absent in BGFC-0.1. The magnified XRD pattern of GdCu-doped BFO between $2\theta = 30$ to 34^{o} is shown in Figure 2(b). It can be observed that the (104) and (110) planes shifted towards a higher angle direction, and a single peak was formed from a merging of two peaks.

3.2. Surface Morphology Analysis

FE-SEM combined with EDAX was used to evaluate the surface morphology and elemental composition. Figure 3(a-n) shows the prepared pure BFO, Gd-doped BFO (BGF-0.1, BGF-0.15, and BGF-0.2), and GdCu-doped BFO (BGFC-0.05, BGFC-0.1, and BGFC-0.15) along with the associated FE-SEM and EDAX results. Based on the FE-SEM images, it was observed that the pure BFO and Gd-doped BFO samples had irregular shapes, and GdCu-doped BFO samples showed a small size of spherical shape. The EDAX analysis confirmed the presence of Bi, Fe, O, Gd, and Cu elemental compositions in the pure BFO and respective doping samples.

Further morphology analysis and particle size distribution were done by TEM. According to Figure 4(a-n), the spherical-shaped particles with small agglomerations were observed. The particle

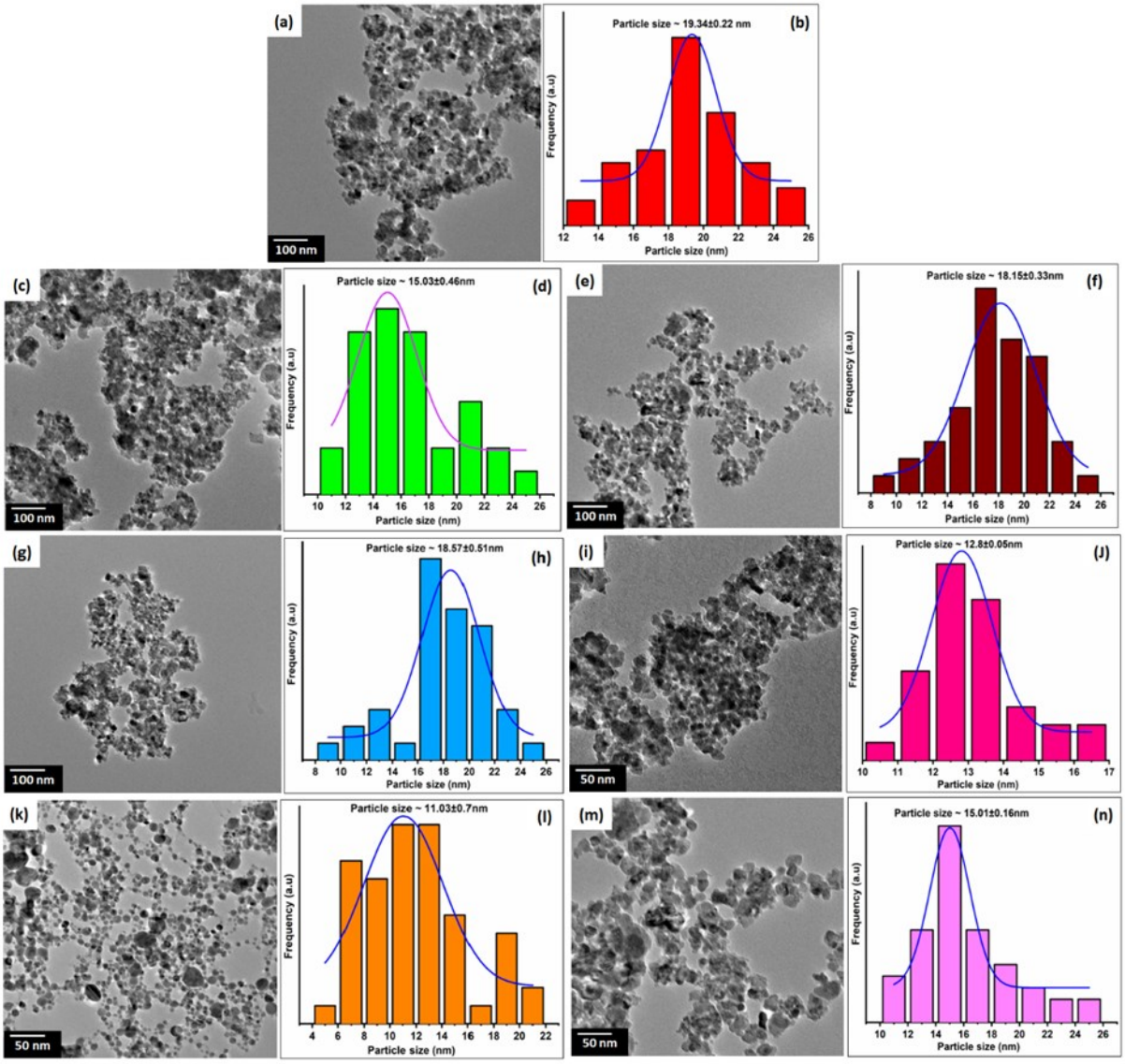

Figure 4. TEM images and particle size distribution of (a-h) pure BFO, BGF-0.1, BGF-0.15, BGF-0.2, (i-n) BGFC-0.05, BGFC-0.1, and BGFC-0.15.

Table 1. A comparison of the research reports on the photocatalytic performance of different materials.

Material doped to $BiFeO_3$	Type of synthesis	Light source	Type of dye	Degradation times (min)	Reference
Cu and Mg	Sol-gel	Visible	Rhodamine B	90	[13]
Gd	Sol-gel	Visible	Rhodamine B	120	[27]
Cu	Co-perpetration	Visible	Methyl orange	120	[28]
Cu	Sol-gel	------	Phenol	120	[29]
Gd	Sol-gel	Visible	Rhodamine B	60	[30]
La and Se	Co-perpetration	Visible	Congo red	30	[33]
Gd and Cu	Sol-gel	Visible	Rhodamine-B	30	Present

size of pure BFO was found to be 19.0 nm and for Gd-doped BFO samples BGF-0.1, BGF-0.15, and BGF-0.2 were 15.0, 18.0, and 18.5 nm respectively. Similarly, for GdCu-doped BFO samples BGFC-0.05, BGFC-0.1 BGFC-0.15 at 12.8, 11.0, and 15.0 nm, respectively.

3.3. Photocatalytic Activity

The photocatalytic activity of BFO, BGF-0.1, BGF-0.15, BGF-0.2, BGCF-0.05, BGCF-0.1, and BGCF-0.15 samples was evaluated by degradation of the typical organic contaminate RhB dye under visible light irradiation and time-dependent photodegradation of RhB is illustrated in Figure 6(a-g). Firstly, stock solution was prepared by using RhB dye 50 mg of pure BFO was added to 100 mL of dye solution to prepare the catalyst solution and it was placed in the dark condition (absence of light) with continuous stirring for 60 min to reach the equilibrium between the dye solution and the catalyst. Next, the catalyst solution was kept under visible light irradiation with continuous stirring, and a small number of samples were collected with equal time intervals up to complete degradation. This was achieved at 160 min for pure BFO and is shown in Figure 6(a). Further, the same procedure was carried out using BGF-0.1, BGF-0.15, and BGF-0.2, and degradation times were observed as 80, 90, and 105 min respectively as shown in Figure 6(b-d). Further research continued for only Gd (0.1wt.%), as BGF-0.1 achieved complete degradation in less time (80 min) in comparison to BGF-0.15, and BGF-0.2. After performing the same procedure on BGFC-0.05, BGFC-0.1, and BGFC-0.15, the degradation times were identified as 60, 30, and 40 min respectively as shown in Figure 6(e-g). As per the results, the Gd (0.1 wt.%) and Cu (0.1 wt.%)-doped BGF-0.1 sample that is BGFC-0.1 has given the best removal of RhB dye with less time (30 min) as compared to other samples (BGFC -0.05, BGFC-0.15) [32]. Table 1 illustrates the summary of available research reports on the photocatalytic activity of various transition and rare -earth materials.

3.4. Photocatalytic Mechanism

It is known that the main factors influencing photocatalytic activity are the generation, separation, transportation, and recombination of photogenerated electron–hole pairs. The quick recombination of electrons and holes in pure BFO is a major problem, causing a low photocatalytic activity. To solve this problem, the recombination of electrons and holes must be avoided. Compared to pure BFO, the GdCu-doped BFO reduces charge recombination, resulting in a longer lifetime of photogenerated electron–hole pairs. Figure 5 demonstrates how the GdCu-doped BFO catalyst degrades the RhB dye when exposed to visible light. As shown in equation (1), the electrons exited from the valance band to the conduction band when visible light rays incident the mixture of catalyst and dye solution. This mechanism typically results in the existence of electrons with a reduction process in the conduction band and holes with an oxidation process in the valence band. From equation (2), reduced (O^{2-}) molecules are created when the oxygen (O_2) molecules in the air capture electrons in the conduction band. In the same way, $^{\cdot}OH$ radicals are created when the hole in the

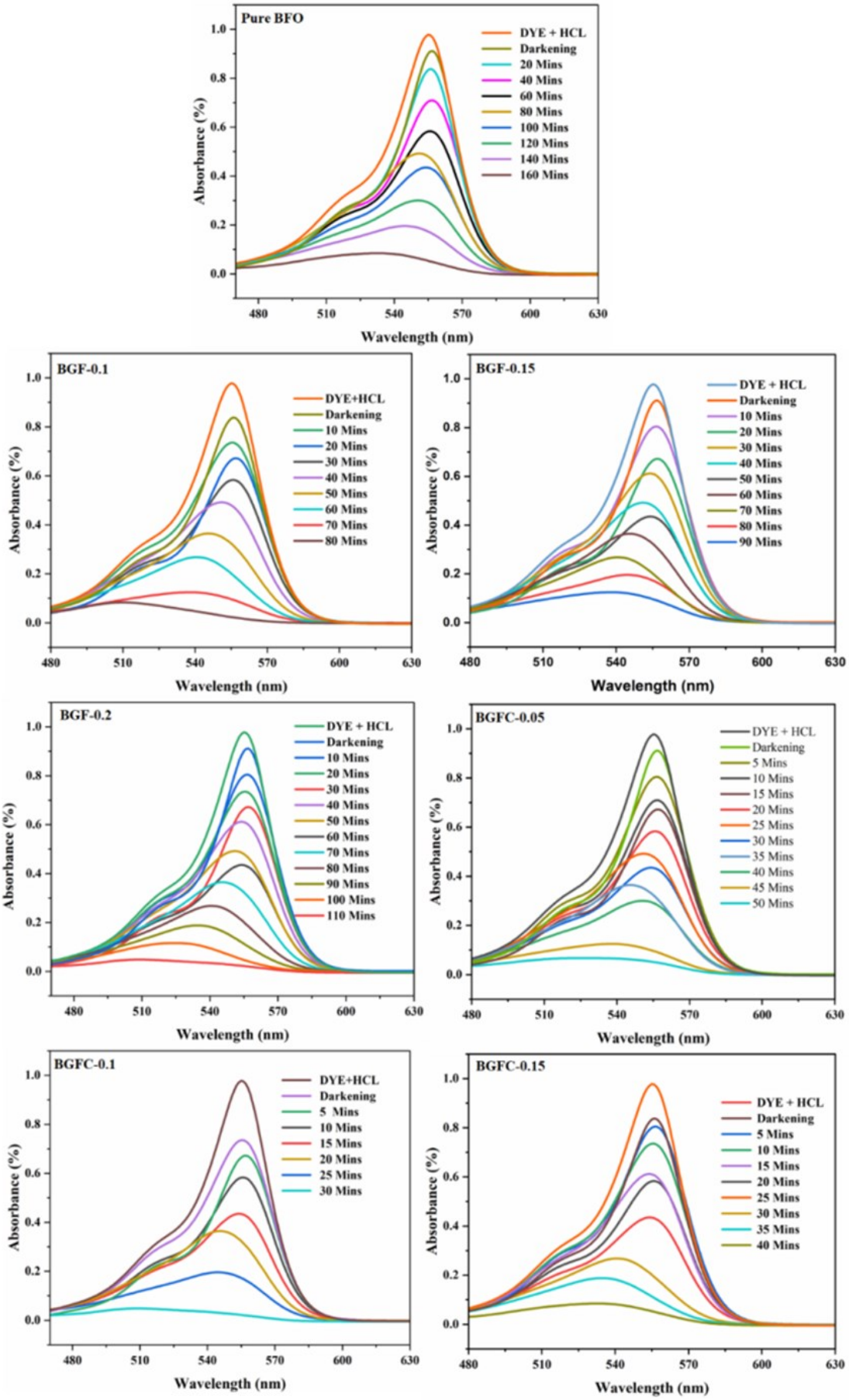

Figure 6. Photocatalytic degradation of RhB dye of pure BFO, BGF-0.1, BGF-0.15, BGF-0.2, BGFC-0.05, BGFC-0.1, and BGFC-0.15.

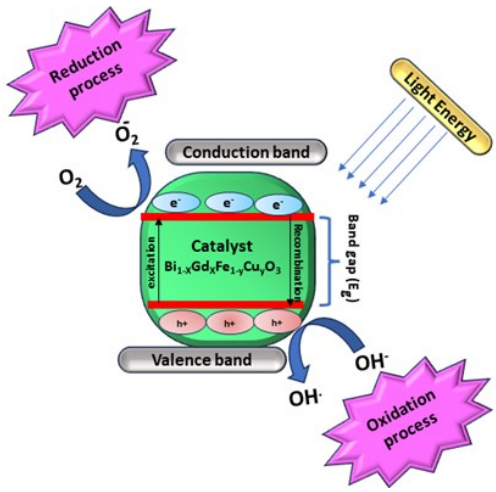

Figure 5. The operational mechanism of the $Bi_{1-x}Gd_xFe_{1-y}Cu_yO_3$ catalyst in the context of degrading Rhodamine B dye under visible light irradiation.

valence band reacts with water molecules on the catalyst surface as shown in equation (3). These two species (O_2^- and ·OH) play a significant role in the degradation of RhB as explained in equations (4) and (5).

$Bi_{1-x}Gd_xFe_{1-y}Cu_yO_3 + h\nu \longrightarrow e^- + h^+$ **(1)**

$e^- + O_2 \longrightarrow O_2^-$ **(2)**

$h^+ + H_2O \longrightarrow OH·$ **(3)**

Catalyst + RhB + OH· —> degradation product **(4)**

Catalyst + RhB + O_2^- —> degradation product **(5)**

4. CONCLUSIONS

In this study, the sol-gel synthesis method was employed to prepare pure BFO and GdCu-doped BFO with different mass percentages. The prepared samples were successfully characterized through XRD, FE-SEM with EDAX, and TEM. The results of XRD analysis revealed that small impurities peaks were formed for both pure BFO and Gd-doped BFO. On the other hand, for GdCu-doped BFO (BGFC-0.05, BGFC-0.1, and BGFC-0.15) samples also showed small impurities peaks expected for BGFC-0.1. FE-SEM and TEM results confirmed that the shape of the particles spherical in shape and size decreased from 19 nm (pure BFO) to 11 nm (BGFC-0.1). The results of photocatalytic activity for RhB dye under visible light irradiation found that the highest degradation performance was achieved for both GdCu-doped BFO (BGFC-0.1) compared to pure BFO, Gd-doped BFO, and GdCu -doped BFO with 0.05 wt.% and 0.15 wt.%.

AUTHOR INFORMATION

Corresponding Author

Padma Suvarna — Department of Physics, Jawaharlal Nehru Technological University Ananthapur, Ananthapuramu-515002 (India);

orcid.org/0000-0002-0543-9034

Email: Padmajntua@gmail.com

Author

Beerelli Rajitha — Department of Physics, Jawaharlal Nehru Technological University Ananthapur, Ananthapuramu-515002 (India);

orcid.org/0000-0002-9787-5959

Author Contributions

All the Authors are equally contributed in Experimentation, characterization and manuscript writing.

Conflicts of Interest

The author(s) declare no conflict of interest.

ACKNOWLEDGEMENT

The author is thankful to Centre for Nano Science &Technology, University of Engineering Science & Technology, JNTU Hyderabad & University of Hyderabad & Osmania University for providing lab and instrumentation facility.

REFERENCES

[1] M. Rashid, W. Hassan, M. Aadil, H. H. Somaily, N. M. Mahdi, R. Lataef, A. G. Taki, K. Srithilat, D. F. Baamer, S. M. Albukhari, M. A. Salam, and A. llyas. (2023). "Solar-light-driven and magnetically recoverable doped nano-ferrite: An ideal photocatalyst for water purification applications". *Optical Materials.* **135**. 10.1016/j.optmat.2022.113192.

[2] P. R. Yaashikaa and P. S. Kumar. (2022). "Fabrication and characterization of magnetic nanomaterials for the removal of toxic pollutants from water environment: A review". *Chemosphere.* **303** (Pt 2): 135067. 10.1016/j.chemosphere.2022.135067.

[3] X. Qu, D. Xie, L. Cao, and F. Du. (2014). "Synthesis and characterization of TiO2/ ZrO2 coaxial core–shell composite nanotubes for photocatalytic applications". *Ceramics International.* **40** (8): 12647-12653. 10.1016/j.ceramint.2014.04.111.

[4] M. Aadil, A. Rahman, S. Zulfiqar, I. A. Alsafari, M. Shahid, I. Shakir, P. O. Agboola, S. Haider, and M. F. Warsi. (2021). "Facile synthesis of binary metal substituted copper oxide as a solar light driven photocatalyst and antibacterial substitute". *Advanced Powder Technology.* **32** (3): 940-950. 10.1016/j.apt.2021.01.040.

[5] Y. Chen, T. Liu, C. Chen, W. Guo, R. Sun, S. Lv, M. Saito, S. Tsukimoto, and Z. Wang. (2013). "Synthesis and characterization of CeO2 nano-rods". *Ceramics International.* **39** (6): 6607-6610. 10.1016/j.ceramint.2013.01.096.

[6] A. Bashir, L. A. Malik, S. Ahad, T. Manzoor, M. A. Bhat, G. N. Dar, and A. H. Pandith. (2018). "Removal of heavy metal ions from aqueous system by ion-exchange and biosorption methods". *Environmental Chemistry Letters.* **17** (2): 729-754. 10.1007/s10311-018-00828-y.

[7] Y. Fu, P. Xu, D. Huang, G. Zeng, C. Lai, L. Qin, B. Li, J. He, H. Yi, M. Cheng, and C. Zhang. (2019). "Au nanoparticles decorated on activated coke via a facile preparation for efficient catalytic reduction of nitrophenols and azo dyes". *Applied Surface Science.* **473** : 578-588. 10.1016/j.apsusc.2018.12.207.

[8] J. Wang and H. Chen. (2020). "Catalytic ozonation for water and wastewater treatment: Recent advances and perspective". *Science of The Total Environment.* **704** : 135249. 10.1016/j.scitotenv.2019.135249.

[9] A. Aziz, F. Basheer, A. Sengar, Irfanullah, S. U. Khan, and I. H. Farooqi. (2019). "Biological wastewater treatment (anaerobic-aerobic) technologies for safe discharge of treated slaughterhouse and meat processing wastewater". *Science of The Total Environment.* **686** : 681-708. 10.1016/j.scitotenv.2019.05.295.

[10] M. d. l. Á. Bernal-Romero del Hombre Bueno, N. Boluda-Botella, and D. Prats Rico. (2019). "Removal of emerging pollutants in water treatment plants: adsorption of methyl and propylparaben onto powdered activated carbon". *Adsorption.* **25** (5): 983-999. 10.1007/s10450-019-00120-7.

[11] N. Rosman, W. N. W. Salleh, M. A. Mohamed, J. Jaafar, A. F. Ismail, and Z. Harun. (2018). "Hybrid membrane filtration-advanced oxidation processes for removal of pharmaceutical residue". *Journal of Colloid and Interface Science.* **532** : 236-260. 10.1016/j.jcis.2018.07.118.

[12] B. Rajitha, K. V. Rao, and R. P. Suvarna. (2020). "Synthesis of multiferroic BiFeO3 microcrystals for photocatalytic activity and stability performance". *Materials Today: Proceedings.* **26** : 126-129. 10.1016/j.matpr.2019.06.325.

[13] R. Beerelli, R. Vanga, and P. Suvarna. (2023). "Effect of Copper doped and Magnesium co-doped BiFeO3 for photocatalytic activity". *Journal of Water and Environmental Nanotechnology.* **8** (3): 285-292. 10.22090/JWENT.2023.03.007.

[14] W. Guo, M. Fu, C. Zhai, and Z. Wang. (2014). "Hydrothermal synthesis and gas-sensing properties of ultrathin hexagonal ZnO nanosheets". *Ceramics International.* **40** (1): 2295-2298. 10.1016/j.ceramint.2013.07.150.

[15] J. Wang, W. Zeng, and Z. Wang. (2016). "Assembly of 2D nanosheets into 3D flower-like NiO: Synthesis and the influence of petal thickness on gas-sensing properties". *Ceramics International.* **42** (3): 4567-4573. 10.1016/j.ceramint.2015.11.150.

[16] F. Davar and M. R. Loghman-Estarki. (2014). "Synthesis and optical properties of pure monoclinic zirconia nanosheets by a new precursor". *Ceramics International.* **40** (6): 8427-8433. 10.1016/j.ceramint.2014.01.052.

[17] L. Renuka, K. S. Anantharaju, S. C. Sharma, H. Nagabhushana, Y. S. Vidya, H. P. Nagaswarupa, and S. C. Prashantha. (2017). "A comparative study on the structural, optical, electrochemical and photocatalytic properties of ZrO2 nanooxide synthesized by different routes". *Journal of Alloys and*

Compounds. **695** : 382-395. 10.1016/j.jallcom.2016.10.126.

[18] E. S. Agorku, A. T. Kuvarega, B. B. Mamba, A. C. Pandey, and A. K. Mishra. (2015). "Enhanced visible-light photocatalytic activity of multi-elements-doped ZrO2 for degradation of indigo carmine". *Journal of Rare Earths.* **33** (5): 498-506. 10.1016/s1002-0721(14)60447-6.

[19] A. Fakhri, S. Behrouz, I. Tyagi, S. Agarwal, and V. K. Gupta. (2016). "Synthesis and characterization of ZrO2 and carbon-doped ZrO2 nanoparticles for photocatalytic application". *Journal of Molecular Liquids.* **216** : 342-346. 10.1016/j.molliq.2016.01.046.

[20] M. Khaksar, M. Amini, D. M. Boghaei, K. H. Chae, and S. Gautam. (2015). "Mn-doped ZrO2 nanoparticles as an efficient catalyst for green oxidative degradation of methylene blue". *Catalysis Communications.* **72** : 1-5. 10.1016/j.catcom.2015.08.023.

[21] M. Sase. (2008). "Enhancement of oxygen exchange at the hetero interface of (La,Sr) CoO3/(La,Sr)2CoO4 in composite ceramics". *Solid State Ionics.* **178** (35-36): 1843-1852. 10.1016/j.ssi.2007.11.039.

[22] M. Rhodes and A. Bell. (2005). "The effects of zirconia morphology on methanol synthesis from CO and H2H2 over Cu/ZrO2Cu/ZrO2 catalystsPart I. Steady-state studies". *Journal of Catalysis.* **233** (1): 198-209. 10.1016/j.jcat.2005.04.026.

[23] Y. Jia, C. Wu, D.-H. Kim, B. W. Lee, S. J. Rhee, Y. C. Park, C. S. Kim, Q. J. Wang, and C. Liu. (2018). "Nitrogen doped BiFeO3 with enhanced magnetic properties and photo-Fenton catalytic activity for degradation of bisphenol A under visible light". *Chemical Engineering Journal.* **337** : 709-721. 10.1016/j.cej.2017.12.137.

[24] Y. Huo, Y. Jin, and Y. Zhang. (2010). "Citric acid assisted solvothermal synthesis of BiFeO3 microspheres with high visible-light photocatalytic activity". *Journal of Molecular Catalysis A: Chemical.* **331** (1-2): 15-20. 10.1016/j.molcata.2010.08.009.

[25] T. Xian, H. Yang, J. F. Dai, Z. Q. Wei, J. Y. Ma, and W. J. Feng. (2011). "Photocatalytic properties of BiFeO3 nanoparticles with different sizes". *Materials Letters.* **65** (11): 1573-1575. 10.1016/j.matlet.2011.02.080.

[26] Y. Liu, R. Zuo, and S. Qi. (2013). "Controllable preparation of BiFeO3@carbon core/shell nanofibers with enhanced visible photocatalytic activity". *Journal of Molecular Catalysis A: Chemical.* **376** : 1-6. 10.1016/j.molcata.2013.04.005.

[27] R. Guo, L. Fang, W. Dong, F. Zheng, and M. Shen. (2010). "Enhanced Photocatalytic Activity and Ferromagnetism in Gd Doped BiFeO3 Nanoparticles". *The Journal of Physical Chemistry C.* **114** (49): 21390-21396. 10.1021/jp104660a.

[28] B. Samran, P. Krongkitsiri, and S. Chaiwichian. (2018). "Effect of Copper Dopants on Visible-Light-Driven Photocatalytic Activity of BiFeO3 Photocatalysts". *Modern Environmental Science and Engineering.* **4** : 234-243. 10.15341/mese(2333-2581)/03.04.2018/006.

[29] J. Mao, X. Quan, J. Wang, C. Gao, S. Chen, H. Yu, and Y. Zhang. (2018). "Enhanced heterogeneous Fenton-like activity by Cu-doped BiFeO3 perovskite for degradation of organic pollutants". *Frontiers of Environmental Science & Engineering.* **12** (6). 10.1007/s11783-018-1060-9.

[30] P. R. B, H. Cui, C. S. M, S. V. P. Vattikuti, Y. Suh, and S.-H. Park. (2019). "Influence of Gd doping on the visible-light photocatalytic activity and magnetic properties of BiFeO3 particles". *Materials Research Express.* **6** (11). 10.1088/2053-1591/ab463d.

[31] N. Tian, Y. Zhang, H. Huang, Y. He, and Y. Guo. (2014). "Influences of Gd Substitution on the Crystal Structure and Visible-Light-Driven Photocatalytic Performance of Bi2WO6". *The Journal of Physical Chemistry C.* **118** (29): 15640-15648. 10.1021/jp500645p.

[32] R. Beerelli, R. Vanga, and R. P. Suvarna. (2023). "Influence of rare earth (Gd) and transition (Cu) doping in bismuth ferrite for photocatalytic activity and stability performance". *Research Square.* 10.21203/rs.3.rs-3099139/v1.

[33] M. Umar, N. Mahmood, S. U. Awan, S. Fatima, A. Mahmood, and S. Rizwan. (2019).

"Rationally designed La and Se co-doped bismuth ferrites with controlled bandgap for visible light photocatalysis". *RSC Advances.* **9** (30): 17148-17156. 10.1039/c9ra03064f.